Dislocations in $SrTiO_3$: easy to reduce but not so fast for oxygen transport

Dario Marrocchelli[1], Lixin Sun[1] and Bilge Yildiz[1,2]*

[1]*Laboratory for Electrochemical Interfaces, Department of Nuclear Science and Engineering, Massachusetts Institute of Technology, 77 Massachusetts Ave., Cambridge, MA 02139, USA*

[2]*Department of Materials Science and Engineering, Massachusetts Institute of Technology, 77 Massachusetts Avenue, Cambridge, MA 02139, USA*

**byildiz@mit.edu*

Supporting Info

1. Interionic potential: parameters and testing

1.1. Parameters of the inter-ionic potential

In this work we used the Thomas interionic potential, reported in ref. [1]. The employed parameters are summarized in Table 1. This potential has been shown to reproduce a large number of experimental properties of $SrTiO_3$, as can be found in refs. [1–8]. This potential has not been used to study reduced $SrTiO_3$, with the exception of ref. [8]. In our work, the extra electrons released upon reduction are distributed between the remaining oxygen and titanium atoms, according to equations 2a and 2b in the paper. This approach is different from the work of Schie et al [8]. In what follows, we validate this approach by performing a series of tests on the chemical expansion, diffusion properties and vacancy formation energy of dislocation-free bulk $SrTiO_3$. We also calculate the dielectric constant of stoichiometric $SrTiO_3$ and show that this is underestimated compared to the experimental value.

	A_{ij} (eV)	ρ_{ij} (eV)	q_i/e
Sr-O	1769.51	0.319894	1.84
Ti-O	14567.40	0.197584	2.36
O-O	6249.17	0.231472	-1.40

Supporting Table 1: Parameters of the Born-Mayer potential for $SrTiO_3$, as from ref [1]. Charges belong to the first ion of the pair.

1.2. Chemical expansion in $SrTiO_3$

Chemical expansion is defined as the changes in the lattice parameter of a material upon changes in its chemical composition, in particular the oxygen non-stoichiometry [9]. Here, we use it as a test of the reliability of the potential for reduced $SrTiO_3$. In Supporting Figure 1, we report the lattice parameter from our calculations at 1200 K on dislocation-free bulk $SrTiO_3$, vs the non-stoichiometry, δ, in $SrTiO_{3-\delta}$. We compare it with the results obtained using the charge neutralization approach from Schie et al[8] and with data from static DFT calculations, performed by us.

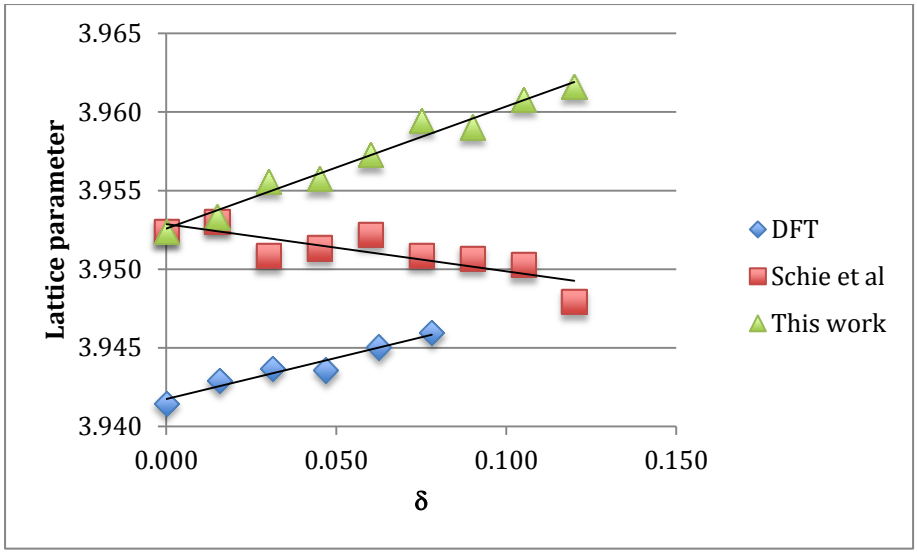

Supporting Figure 1: Latttice parameter vs non-stoichiometry, δ. MD calculations are performed at 1200 K while DFT calculations are at 0 K.

One can clearly see that our results are in good agreement with the DFT calculations in predicting a lattice *expansion* upon reduction of $SrTiO_3$ (i.e. upon the introduction of oxygen vacancies and compensating electrons). The slopes of the curves are very similar both for the DFT results and by using the Thomas interionic potential in this work. The chemical expansion coefficients, extracted by fitting the data in Supporting Figure 1 are reported in the Supporting Table 2. Interestingly, the approach employed by Schie et al yields a negative chemical expansion coefficient. No experimental data reporting chemical expansion coefficients in $SrTiO_3$ is available, though in refs.[10,11] the authors do observe a small expansion upon reduction of La-doped $SrTiO_3$.

Source	Chemical expansion coefficient
DFT (0 K)	0.013
Schie et al (1200 K)	-0.08
Our work (1200 K)	0.020

Supporting Table 2: Chemical expansion coefficients extracted from Supporting Figure 1.

1.3. Oxygen diffusion coefficient vs vacancy concentration

Here we focus on the behavior of *D* (the oxygen diffusion coefficient) versus the vacancy concentration in $SrTiO_3$ (bulk model, without dislocations) at a certain temperature (1200 K). This behavior has been the object of intense study in other perovskite-structured materials (e.g. $LaGaO_3$ [12,13]) as well as other oxides [14,15]. Indeed, it is well known that *D* shows a maximum for a certain critical vacancy concentration and then decreases strongly for higher values of $[V_O^{\cdot\cdot}]$. While to the authors' knowledge no experimental data are available for the behavior of *D* vs $[V_O^{\cdot\cdot}]$ (tracer experiments in $SrTiO_3$ are usually performed only at one or two vacancy concentrations [16,17]), one expects $SrTiO_3$ to behave similarly to other perovskite materials [12,13].

In Supporting Figure 2 we report the oxygen diffusion coefficient vs vacancy concentration for $SrTiO_3$. A clear maximum can be observed for a vacancy concentration of ~ 10 %. We note that the presence of this maximum depends on the way the extra electrons are distributed. Indeed, if the extra electrons are assigned to Ti cations only (either by having Ti^{3+} cations or by sharing the extra electrons equally among all the Ti cations), the ionic conductivity increases indefinitely as $[V_O^{\cdot\cdot}]$ is increased. This further confirms that Equations 2a and b in the main paper represent a reasonable choice for the charge distribution.

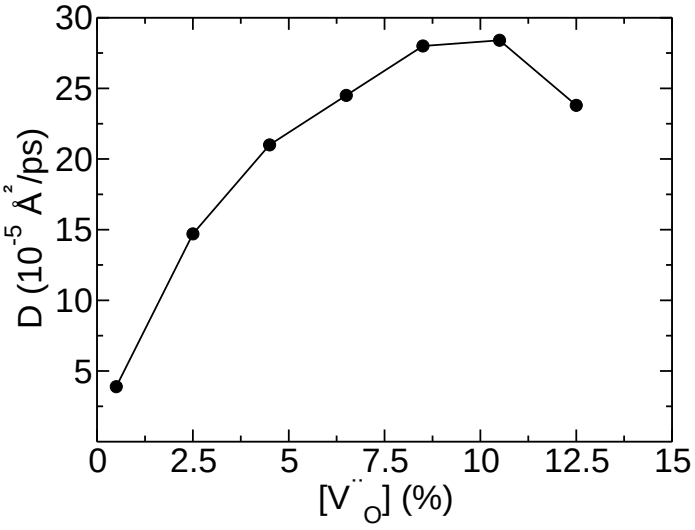

Supporting Figure 2: Diffusion coefficient, D, vs vacancy concentration, $[V_O^{\cdot\cdot}]$, for dislocation-free bulk $SrTiO_3$ at 1200 K.

1.4. Strain effects on the reducibility of $SrTiO_3$

Dislocations introduce strain fields near the core, as mentioned throughout the paper. One is therefore interested in testing the validity of our potential when $SrTiO_3$ is strained. To this end, we calculated the change in the vacancy formation energy for different lattice parameters (corresponding to different values of isotropic strain) in bulk, dislocation-free $SrTiO_3$, and compared it to DFT calculations. Our approach was analogous to that in previous studies on related materials.[18–20] This is reported in Supporting Figure 3, which shows a good agreement between DFT and our calculations.

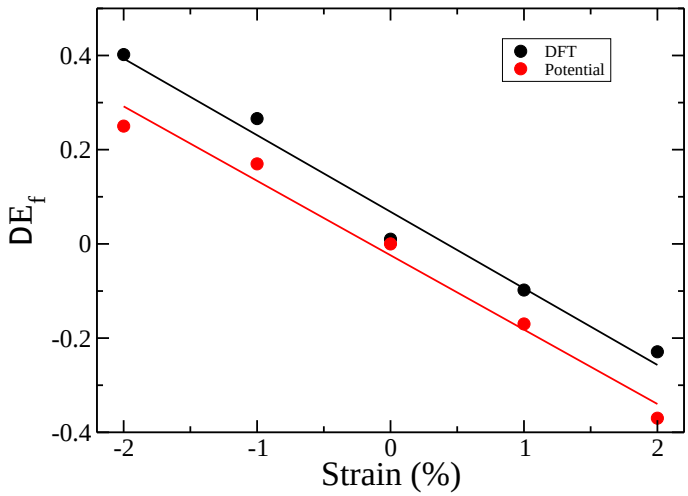

Supporting Figure 3: Variation in the vacancy formation energy in $SrTiO_3$ vs. the applied isotropic strain, calculated by using DFT (black points) and by using the potential in Supporting Table 1 (red points). The solid lines are a linear fit to the data points and are provided as a guide to the eye.

1.5. Dielectric constant calculation

The GULP code[21] was employed to calculate the dielectric constant of stoichiometric $SrTiO_3$. The focus of GULP on analytical solutions makes the calculation of dielectric constants straightforward. The dielectric constant was found to be 4.8, regardless of the employed system size, potential cut-off and input-structure (relaxed vs non-relaxed). We note that this calculation was performed at 0 K, but on a cubic $SrTiO_3$ to represent its crystal structure at room temperature. A comparison with the experimental dielectric constant[22] of ~300 at room temperature shows that the potential in Supporting Table 1 cannot reproduce the dielectric constant well. This limitation was briefly discussed by Thomas et al. in ref. [1], where they say that this has to do with poorly predicted soft modes. Other properties calculated with GULP, such as bulk modulus, elastic constants, shear modulus, Poisson ratio, Young modulus and cohesive energy, are in line with experimental values,[1,23] and are identical to those obtained in LAMMPS.

2. Diffusion Coefficient Calculation

In this work diffusion coefficients are extracted from the slope of the mean squared displacement (MSD) of the ionic species of interest [14,15,24–26]. When studying bulk $SrTiO_3$ (with no dislocations), all the oxygen ions are included in the MSD calculation. For simulation boxes with dislocations, we define a series of regions, as schematically shown in Figure 6 (a) of the paper. The MSD of these atoms is then calculated, so that we can extract the diffusion coefficient of oxygen atoms from these specific regions and thus study any effect of the dislocation core on the oxide-ion diffusivity. For each dislocation core, we define the following regions: a dislocation core region (purple circle) and three rim regions in the compressive/tensile part above/below the core, at different distances from the core. We also define two bulk-like regions that are 5 nm above/below the core, where we expect the system to be uniaxially strained along the y-axis (because of the removal of atomic planes and periodic boundary conditions, see Figure 1 (b)) but otherwise unaffected by the dislocation core. Since we have two *identical* dislocations in our simulations, we average the diffusion coefficients coming from analogous zones of the two dislocations. This allows to simulate more atoms in each of the regions defined above, thus improving significantly the statistics. Our simulations were in the 900-1500 K temperature range and the trajectories lasted up to 30 ns. Lower temperatures could not be studied because the dynamics is too slow for time-scales of reach to Molecular Dynamics simulations.

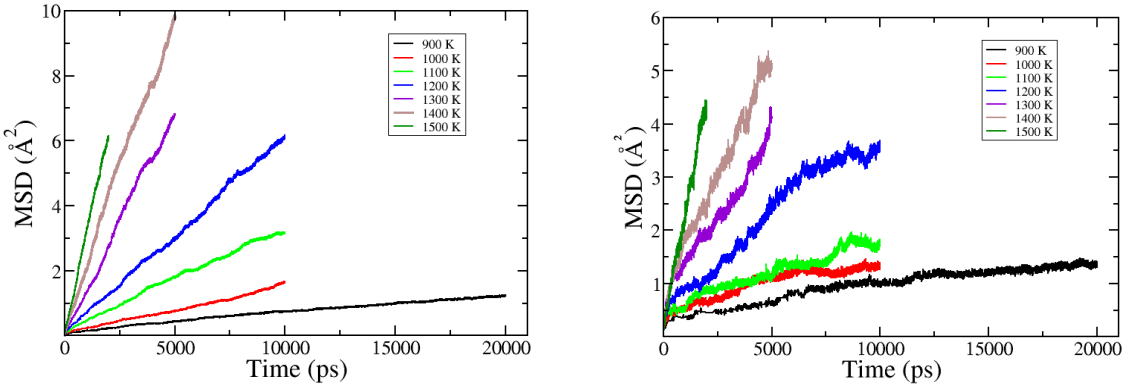

Supporting Figure 4: Mean Squared Displacements (MSD) of the oxygen ions in the tensile region next to the dislocation (left) and at the dislocation core (right), in 2.5% oxygen deficient $SrTiO_3$ for different temperatures.

In most cases, each region defined in Figure 6 (a) contains 3,000-15,000 oxide ions and the corresponding MSD curves are straight and smooth (see Supporting Figure 4), so that reliable diffusion coefficients can be extracted. In these cases, we have estimated the error associated with the diffusion coefficients (by fitting MSD curves of different lengths) to be ~ 5%, similar to previous work [24]. The only exception is the core region which contains only ~300 atoms. The corresponding MSD curves are noisier (see Supporting Figure 4), which in turn leads to a higher error in the

calculated diffusion coefficient. For this reason, long simulations (30 ns) were performed to improve the statistics and, in certain cases (e.g. sample I and sample II), the diffusion coefficients were averaged over several independent calculations (up to 5). In this case, the error bars were estimated from the standard deviation. For $SrTiO_3$ with 2.5% vacancy concentration, we have also extracted activation energies, by calculating diffusion coefficients at different temperatures (900 – 1500 K). The error associated with the activation energies is ~ 0.05 eV and was estimated from its standard deviation at different temperature ranges. We stress here that these simulations represent the limit of what can be obtained with classical MD simulations nowadays. Indeed, in this study we were able to calculate diffusion coefficients as low as 10^{-11} cm^2/s from regions that contained only a few hundred atoms. This was made possible by 1) using computationally efficient rigid-ion model potentials, 2) using LAMMPS, a software that can be run on hundreds of computing cores with an almost liner scaling performance and 3) by running these calculations on Stampede, the 7th fastest supercomputer in the World. An MD run of 5 ns would use 512 cores for approximately 2 days. A total of ~ 2.0 million CPU hours were used for this project.

3. Vacancy analysis

A simple vacancy analysis code was developed based on the Ti atom coordination. The key idea is that, in a perfect perovskite structure, there are 6 oxygens around one Ti cation. If an oxygen vacancy (or several oxygen vacancies) is near a Ti cation, then the cation coordination number will be less than 6. By calculating the average Ti coordination number in one region, one can extract the local oxygen vacancy concentration. By way of example, in Supporting Figure 5 (a), we report only those Ti cations that have a coordination number lower than 6 in sample I (which has 0.017% vacancy concentration). One can clearly see that the only under-coordinated cations are in the vicinity of the dislocation cores. We note that this under-coordination stems both from the presence of oxygen vacancies at the core and from the fact that Ti cations are under-coordinated in the vicinity of the core, because of its different structure. In conclusion, supporting Figure 5 (a) shows, unequivocally, that there are no oxygen vacancies in the bulk of the system.

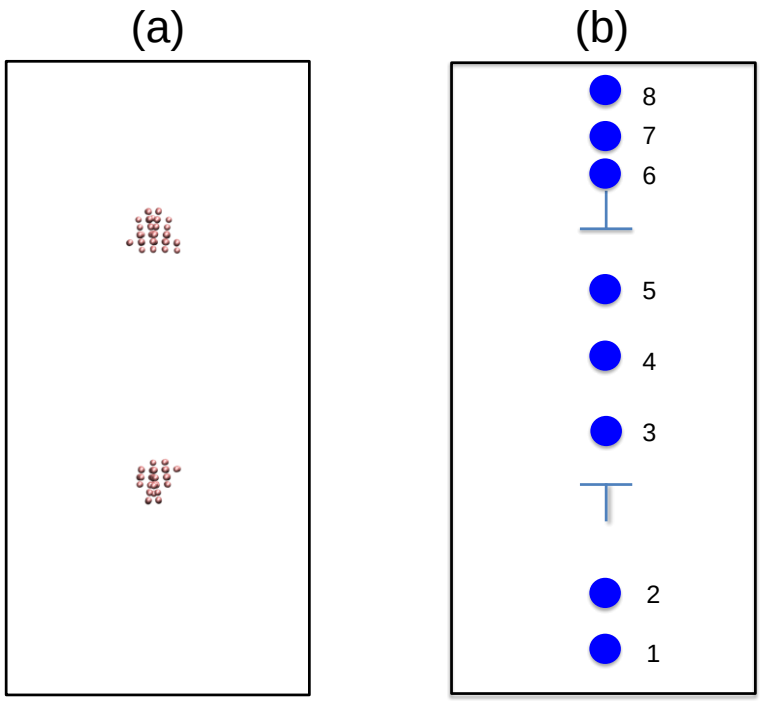

*Supporting Figure 5: (a) Under-coordinated Ti atoms in sample I (*0.017% vacancy concentration at 1200 K*) after 10 ns. There is no evidence of under-coordinated Ti atoms in regions away from the two dislocations, thus confirming that vacancies are bound at the dislocation cores. Similar figures are obtained after 30 ns. (b) Schematic showing the 8 regions*

sampled for the vacancy concentration calculation in $SrTiO_3$ with an average oxygen vacancy concentration of 2.5% at the end of a 10 ns run at 1200 K.

This vacancy analysis technique has also been used to probe local variations in the oxygen vacancy concentration for $SrTiO_3$ with 2.5% vacancy concentration at 1200 K. Supporting Figure 5 (b) shows a schematic of the 8 regions that we sampled. The respective oxygen vacancy concentrations are reported in Supporting Table 2. These reported values are all quite close to the total vacancy concentration (2.5%), confirming that in this case the oxygen vacancies are distributed quite homogeneously.

Position	$[V_O^{\cdot\cdot}]$ (%)
1	3.07
2	2.28
3	2.68
4	2.77
5	2.58
6	2.70
7	2.62
8	2.62

Supporting Table 3: Calculated vacancy concentration for the regions shown in Supporting Figure 5 (b).

4. How many vacancies can be trapped at dislocations in $SrTiO_3$?

By knowing that dislocations (defined as tubes with a 0.4 nm diameter) can accommodate 8% vacancy concentration (see section 3.2 of our paper) and by knowing the dislocation density and vacancy concentration in real samples, one can estimate how many vacancies will be trapped near dislocations. This can be done as follows: using the dislocation density and the area of one individual dislocation ($\pi r^2 \sim 0.5$ nm^2), one can calculate the percentage area of the material occupied by the dislocation cores. This quantity is displayed in the third column of *Supporting Table **4***, as a percentage. It can be seen that, even when their density is high, dislocations only occupy a tiny area of the sample (less than 0.003%). From this quantity, assuming these dislocations can contain 8% vacancies, one can estimate how many vacancies are trapped at the cores. This is reported in column 4 of *Supporting Table **4***. Interestingly, in materials with high dislocation densities ($\sim 5 \times 10^9$ cm^{-2}), dislocation can accommodate a few ppm of vacancies which, in certain cases, can be a significant fraction of the total number of vacancies (in ref. [16] they estimate [V] ~ 7 ppm).

Disl. Density	Core Area	Total Disl. Area (%)	[V] @ core	[V]	Ref.
4×10^9 cm^{-2}	0.5 nm^2	0.002	1.6 ppm	7 - 200 ppm	[27]
6×10^9 cm^{-2}	0.5 nm^2	0.003	2.4 ppm	7 - 200 ppm	[28]
6×10^7 cm^{-2}	0.5 nm^2	3.0×10^{-5}	0.024 ppm	7 -200 ppm	[16]

Supporting Table 4: Estimate of the number of vacancies that are trapped at dislocations, for different values of dislocation densities, as obtained from the literature.

5. References

(1) Thomas, B. S.; Marks, N. A.; Begg, B. D. *Nucl. Instrum. Methods Phys. Res. Sect. B Beam Interact. Mater. At.* **2005**, *228*, 288.
(2) Benedek, N. A.; Chua, A. L.-S.; Elsässer, C.; Sutton, A. P.; Finnis, M. W. *Phys. Rev. B* **2008**, *78*, 064110.
(3) Chua, A. L.-S.; Benedek, N. A.; Chen, L.; Finnis, M. W.; Sutton, A. P. *Nat. Mater.* **2010**, *9*, 418.
(4) Uberuaga, B. P.; Choudhury, S.; Bai, X.-M.; Benedek, N. A. *Scr. Mater.* **2012**, *66*, 105.
(5) Hirel, P.; Marton, P.; Mrovec, M.; Elsässer, C. *Acta Mater.* **2010**, *58*, 6072.

(6) Hirel, P.; Mrovec, M.; Elsässer, C. *Acta Mater.* **2012**, *60*, 329.
(7) Thomas, B.; Marks, N.; Harrowell, P. *Phys. Rev. B* **2006**, *74*.
(8) Schie, M.; Marchewka, A.; Müller, T.; De Souza, R. A.; Waser, R. *J. Phys. Condens. Matter* **2012**, *24*, 485002.
(9) Bishop, S. R.; Marrocchelli, D.; Chatzichristodoulou, C.; Perry, N. H.; Mogensen, M. B.; Tuller, H. L.; Wachsman, E. D. *Annu. Rev. Mater. Res.* **2013**, *44*, 140228162707002.
(10) Marina, O. A.; Canfield, N. L.; Stevenson, J. W. *Solid State Ion.* **2002**, *149*, 21.
(11) Hashimoto, S.; Kindermann, L.; Larsen, P. H.; Poulsen, F. W.; Mogensen, M. *J. Electroceramics* **2006**, *16*, 103.
(12) Huang, K.; Tichy, R. S.; Goodenough, J. B. *J. Am. Ceram. Soc.* **1998**, *81*, 2565.
(13) Khan, M. S.; Islam, M. S.; Bates, D. R. *J. Phys. Chem. B* **1998**, *102*, 3099.
(14) Marrocchelli, D.; Madden, P. A.; Norberg, S. T.; Hull, S. *Chem. Mater.* **2011**, *23*, 1365.
(15) Burbano, M.; Norberg, S. T.; Hull, S.; Eriksson, S. G.; Marrocchelli, D.; Madden, P. A.; Watson, G. W. *Chem. Mater.* **2012**, *24*, 222.
(16) De Souza, R. A.; Metlenko, V.; Park, D.; Weirich, T. E. *Phys. Rev. B* **2012**, *85*.
(17) Metlenko, V.; Ramadan, A.; Gunkel, F.; Du, H.; Schraknepper, H.; Hoffmann-Eifert, S.; Dittmann, R.; Waser, R.; Souza, R. D. *Nanoscale* **2014**.
(18) Rupp, J. L. M.; Fabbri, E.; Marrocchelli, D.; Han, J.-W.; Chen, D.; Traversa, E.; Tuller, H. L.; Yildiz, B. *Adv. Funct. Mater.* **2014**, *24*, 1562.
(19) Ahn, K.; Chung, Y.-C.; Yoon, K. J.; Son, J.-W.; Kim, B.-K.; Lee, H.-W.; Lee, J.-H. *J. Electroceramics* **2014**, *32*, 72.
(20) De Souza, R. A.; Ramadan, A.; Hörner, S. *Energy Environ. Sci.* **2012**, *5*, 5445.
(21) Gale, J. D. *J. Chem. Soc. Faraday Trans.* **1997**, *93*, 629.
(22) Neville, R. C.; Hoeneisen, B.; Mead, C. A. *J. Appl. Phys.* **1972**, *43*, 2124.
(23) Piskunov, S.; Heifets, E.; Eglitis, R. .; Borstel, G. *Comput. Mater. Sci.* **2004**, *29*, 165.
(24) Burbano, M.; Marrocchelli, D.; Watson, G. W. *J. Electroceramics* **2014**, *32*, 28.
(25) Burbano, M.; Nadin, S.; Marrocchelli, D.; Salanne, M.; Watson, G. W. *Phys. Chem. Chem. Phys.* **2014**, *16*, 8320.
(26) Norberg, S. T.; Hull, S.; Ahmed, I.; Eriksson, S. G.; Marrocchelli, D.; Madden, P. A.; Li, P.; Irvine, J. T. S. *Chem. Mater.* **2011**, *23*, 1356.
(27) Szot, K.; Speier, W.; Carius, R.; Zastrow, U.; Beyer, W. *Phys. Rev. Lett.* **2002**, *88*.
(28) Wang, R.; Zhu, Y.; Shapiro, S. M. *Phys. Rev. Lett.* **1998**, *80*, 2370.